J. Fluid Mech. (1976), *vol.* 77, *part* 4, *pp.* 753–768
Printed in Great Britain

Diffusion of passive-scalar and magnetic fields by helical turbulence

By ROBERT H. KRAICHNAN
Dublin, New Hampshire 03444

(Received 23 March 1976)

Computer simulations of fluid-element trajectories in mirror-symmetric and maximally helical turbulence are used to evaluate Moffatt's (1974) formulae for the magnetic diffusivity $\eta(t)$ and the coefficient $\alpha(t)$ of the alpha-effect. The passive-scalar diffusivity $\kappa(t)$ and the mean response functions of scalar and magnetic field wave-vector modes are also computed. The velocity field is normal, stationary, homogeneous and isotropic with spectrum $E(k) = \frac{3}{2}v_0^2\delta(k-k_0)$ and time correlation $\exp[-\frac{1}{2}\omega_0^2(t-t')^2]$. The cases $\omega_0 = 0$ (frozen turbulence), $\omega_0 = v_0 k_0$ and $\omega_0 = 2v_0 k_0$ are followed to $t = 4/v_0 k_0$. In the $\omega_0 > 0$ cases with maximal helicity, $\eta(t)$ and $\alpha(t)$ approach steady-state values of order v_0/k_0 and v_0, respectively. They behave anomalously for $\omega_0 = 0$. In the mirror-symmetric cases, $\eta(t)$ and $\kappa(t)$ differ very little from each other. At all the ω_0 values, $\kappa(t)$ is bigger in the helical than in the mirror-symmetric case. The difference is marked for $\omega_0 = 0$. The simulation results imply that $\eta(t)$ becomes negative in non-normal mirror-symmetric turbulence with strong helicity fluctuations that persist over several correlation lengths and times. The computations of response functions indicate that asymptotic expressions for these functions, valid for $k \ll k_0$, retain good accuracy for $k \sim k_0$. The mean-square magnetic field is found to grow exponentially, and its kurtosis also grows rapidly with t, indicating rapid development of a highly intermittent distribution of magnetic field.

1. Introduction

Moffatt (1974) has given exact Lagrangian expressions for the coefficient of the α-effect and for the diffusivity experienced by a slowly varying weak magnetic field in a perfectly conducting fluid which is in statistically homogeneous turbulent motion. These expressions, and related formulae for the mean response functions of Fourier modes of the magnetic field, are suited for direct computer simulation. They are thereby a tool for resolving some questions about the behaviour of the magnetic field which have not been convincingly settled by approximate theory.

The present paper reports computer simulations for several examples of helical and reflexion-invariant homogeneous, isotropic, random velocity fields. The technique used is an extension of one previously exploited for the computation of passive-scalar diffusivities (Kraichnan 1970). A large number of fluid-element trajectories are explicitly constructed and the desired diffusivities

and other quantities are computed as averages over the distribution of trajectories. In the case of the magnetic field, it is necessary to follow the strain as well as the displacement of the fluid elements. We do this by tracing the history of closely spaced pairs of fluid elements.

In addition to determining the behaviour of the α-effect coefficient $\alpha(t)$ and the magnetic diffusivity $\eta(t)$ for normally distributed turbulence both with mirror symmetry and with maximal helicity, a principal purpose of the present paper is to test a recent prediction (Kraichnan 1976) that large-scale fluctuations of helicity in non-normal mirror-symmetric flows yield negative values of $\eta(t)$ for sufficiently long times t. We also find the mean response functions of the magnetic field at wavenumbers comparable to those of the velocity field. Finally, we give measures of the intermittency of the magnetic-field fluctuations induced by the turbulence.

2. The basic Lagrangian formulae

A weak magnetic field in a perfectly conducting incompressible fluid obeys

$$\partial B_i/\partial t = \partial(u_i B_j - u_j B_i)/\partial x_j, \tag{2.1}$$

with

$$\nabla.\mathbf{B} = \nabla.\mathbf{u} = 0. \tag{2.2}$$

Here $\mathbf{B}$ and $\mathbf{u}$ are the total magnetic field and total velocity field, respectively. The general solution of (2.1) can be written as

$$B_i(\mathbf{X}(\mathbf{a},t),t) = B_j(\mathbf{a},0)\,\partial \mathbf{X}_i/\partial a_j, \tag{2.3}$$

where $\mathbf{X}(\mathbf{a},t)$ is the position at time t of the fluid element located at $\mathbf{a}$ when $t = 0$.

If $\mathbf{u}$ is a turbulent velocity field, and the initial magnetic field is statistically independent of the velocity field, then the ensemble-averaged magnetic field obeys a differential equation which, in the homogeneous isotropic case, has the form

$$\partial\langle\mathbf{B}(\mathbf{x},t)\rangle/\partial t = -\alpha(t)\,\nabla\times\langle\mathbf{B}(\mathbf{x},t)\rangle + \eta(t)\,\nabla^2\langle\mathbf{B}(\mathbf{x},t)\rangle + \ldots. \tag{2.4}$$

The higher terms in (2.4) involve spatial derivatives of $\langle\mathbf{B}(\mathbf{x},t)\rangle$ of higher than second order and are negligible if the time and space scales of variation of $\langle\mathbf{B}(\mathbf{x},t)\rangle$ are large compared with any correlation scale of the turbulence. The coefficients $\alpha(t)$ and $\eta(t)$ can be directly found from (2.3) by making a spatial Taylor expansion of the initial mean magnetic field (Moffatt 1974). They can be written compactly in the form (Kraichnan 1976)

$$\alpha(t) = d\gamma(t)/dt, \quad \eta(t) = d\zeta(t)/dt + \tfrac{1}{2}d[\gamma(t)]^2/dt, \tag{2.5}$$

where

$$\gamma(t) = \tfrac{1}{6}\langle\epsilon_{inj}\,\xi_n(t)\,\partial X_i(t)/\partial a_j\rangle, \tag{2.6}$$

$$\zeta(t) = \tfrac{1}{15}[2\langle\xi_i(t)\,\xi_i(t)\,\partial X_n(t)/\partial a_n\rangle - \langle\xi_i(t)\,\xi_n(t)\,\partial X_i(t)/\partial a_n\rangle]. \tag{2.7}$$

In these equations, $\xi_i(\mathbf{a},t) = X_i(\mathbf{a},t) - a_i$ and the argument $\mathbf{a}$ is implicit.

The quantities $\alpha(t)$, $\eta(t)$, $\gamma(t)$ and $\zeta(t)$ can be written in a variety of ways by using isotropy properties and the homogeneity property that the derivative of any average with respect to $\mathbf{a}$ vanishes. Thus it can be found that

$$\zeta(t) = \tfrac{1}{6}\langle|\boldsymbol{\xi}|^2(1 + \tfrac{1}{2}\partial\xi_i/\partial a_i)\rangle. \tag{2.8}$$

The expressions which we shall actually use for computation in this paper are

$$\gamma(t) = \tfrac{1}{2}\langle(\xi_3\,\partial\xi_2/\partial a_1) - (\xi_2\,\partial\xi_3/\partial a_1)\rangle, \tag{2.9}$$

$$\alpha(t) = \langle(v_3\,\partial\xi_2/\partial a_1) - v_2\,\partial\xi_3/\partial a_1)\rangle, \tag{2.10}$$

$$\zeta(t) = \tfrac{1}{4}\langle(\xi_2^2+\xi_3^2)\,\partial X_1/\partial a_1\rangle, \tag{2.11}$$

$$d\zeta(t)/dt = \tfrac{1}{2}\langle(\xi_2 v_2+\xi_3 v_3)\,\partial X_1/\partial a_1\rangle + \tfrac{1}{4}\langle(\xi_2^2+\xi_3^2)\,\partial v_1/\partial a_1\rangle. \tag{2.12}$$

Here $v_i(\mathbf{a},t) = d\xi_i(\mathbf{a},t)/dt$ is the Lagrangian velocity and v_1, v_2 and v_3 are components along the axes of a right-handed Cartesian system.

The corresponding relations for a passively advected scalar field are

$$\partial\phi/\partial t + u_i\,\partial\phi/\partial x_i = 0, \tag{2.13}$$

$$\phi(\mathbf{X}(\mathbf{a},t),t) = \phi(\mathbf{a},0), \tag{2.14}$$

$$\partial\langle\phi(\mathbf{x},t)\rangle/\partial t = \kappa(t)\,\nabla^2\langle\phi(\mathbf{x},t)\rangle, \tag{2.15}$$

$$\kappa(t) = d\Xi(t)/dt, \quad \Xi(t) = \tfrac{1}{6}\langle\xi_i(t)\,\xi_i(t)\rangle. \tag{2.16}$$

Isotropy and homogeneity imply that the mean response tensor for a wave-vector mode of the magnetic field has the form

$$g_{ij}(\mathbf{k},t) = P_{ij}(\mathbf{k})\,g(k,t) + ik_m\,\epsilon_{imj}\,h(k,t), \quad g(k,0) = 1, \quad h(k,0) = 0, \tag{2.17}$$

where

$$P_{ij}(\mathbf{k}) = \delta_{ij} - k_i\,k_j/k^2.$$

To evaluate $g(k,t)$ and $h(k,t)$, we may assume a large cyclic box of volume V and take

$$B_i(x,0) = [\exp(i\mathbf{k}.\mathbf{x}), 0, 0], \tag{2.18}$$

where $\mathbf{k}$ lies in the 2,3 plane. Then, by (2.17) and the definition of a response tensor,

$$\left.\begin{aligned} g(k,t) &= V^{-1}\textstyle\int\langle B_1(\mathbf{x},t)\rangle\exp(-i\mathbf{k}.\mathbf{x})\,d^3x, \\ h(k,t) &= ik^{-1}V^{-1}\textstyle\int\langle B_3(\mathbf{x},t)\rangle\exp(-i\mathbf{k}.\mathbf{x})\,d^3x \quad [\mathbf{k} = (0,k,0)]. \end{aligned}\right\} \tag{2.19}$$

From (2.3) we have

$$\langle B_i(\mathbf{x},t)\rangle = \exp(i\mathbf{k}.\mathbf{x})\langle(\partial X_i/\partial a_1)\exp(-i\mathbf{k}.\boldsymbol{\xi})\rangle_{\mathbf{X}=\mathbf{x}}. \tag{2.20}$$

The notation $\langle\ \rangle_{\mathbf{X}=\mathbf{x}}$ in (2.20) means that the average is over that trajectory, in each realization, which passes through the given point $\mathbf{x}$ at time t. By homogeneity, the average in (2.20) is independent of $\mathbf{x}$. A further consequence of homogeneity is that the average is independent of whether the point $\mathbf{x}$ is kept fixed, as written, or the initial point $\mathbf{a}$ is kept fixed. From (2.19) and (2.20),

$$\left.\begin{aligned} g(k,t) &= \langle(\partial X_1/\partial a_1)\exp(-i\mathbf{k}.\boldsymbol{\xi})\rangle, \\ h(k,t) &= ik^{-1}\langle(\partial X_3/\partial a_1)\exp(-i\mathbf{k}.\boldsymbol{\xi})\rangle. \end{aligned}\right\} \tag{2.21}$$

Additional reduction results from further use of isotropy properties. In the expression (2.21) for $g(k,t)$, the result must be independent of the direction of $\mathbf{k}$ in the 2,3 plane. Averaging over this direction, we have

$$g(k,t) = \langle(\partial X_1/\partial a_1)\,J_0[k(\xi_2^2+\xi_3^2)^{\frac{1}{2}}]\rangle. \tag{2.22}$$

For $h(k,t)$, we take k along the x_2 axis but symmetrize the final expression by exchanging the roles of x_2 and x_3 in (2.19) *et seq.* The result is

$$h(k,t) = \tfrac{1}{2}k^{-1}\langle(\partial X_3/\partial a_1)\sin(k\xi_2) - (\partial X_2/\partial a_1)\sin(k\xi_3)\rangle. \tag{2.23}$$

The sines appear in (2.23) because isotropy implies that the even terms in the expansion of the exponential in the expression (2.21) for $h(k,t)$ do not contribute.

The corresponding expressions for the response function $g_s(k,t)$ of the passive-scalar field are

$$g_s(k,t) = \langle\exp(-i\mathbf{k}.\boldsymbol{\xi})\rangle, \quad g_s(k,t) = \langle\sin(k\xi)/(k\xi)\rangle. \tag{2.24), (2.25}$$

In (2.24), $\mathbf{k}$ has any direction in three dimensions, and (2.25) results from an average over this direction.

The isotropic formulae (2.22)–(2.24) are exact. They do not restrict k to values small compared with the wavenumbers of the turbulence. If k is small compared with any wavenumbers of the turbulence, alternative expressions for the response functions are obtained by integrating (2.4) and (2.15):

$$g(k,t) \approx \exp[-k^2(\zeta+\tfrac{1}{2}\gamma^2)]\cosh(k\gamma) \quad (k \ll k_0), \tag{2.26}$$

$$h(k,t) \approx -\exp[-k^2(\zeta+\tfrac{1}{2}\gamma^2)]\sinh(k\gamma) \quad (k \ll k_0), \tag{2.27}$$

$$g_s(k,t) \approx \exp(-k^2\Xi) \quad (k \ll k_0), \tag{2.28}$$

where k_0 denotes a characteristic wavenumber of the turbulence. If now (2.22), (2.23) and (2.25) are expanded in powers of k the results must be equivalent to the expansions of (2.26)–(2.28), term by term. This implies certain relations among Lagrangian moments, of the displacement and strain fields, for times long compared with turbulence correlation times. We shall discuss them in a later section of the paper.

3. Method of simulation

We compute the Lagrangian formulae of § 2 by a modification of the method used previously for scalar diffusion (Kraichnan 1970). We seek to realize velocity fields whose covariance has the form

$$\langle\mathbf{u}(\mathbf{x}+\mathbf{r},t).\mathbf{u}(\mathbf{x},t')\rangle = 2D(t-t')\int_0^\infty E(k)\frac{\sin(kr)}{kr}dk, \tag{3.1}$$

and which display isotropic, homogeneous, normal statistics. The time correlation function is taken to be of the form

$$D(t-t') = \exp[-\tfrac{1}{2}\omega_0^2(t-t')^2], \tag{3.2}$$

and the spectrum function is taken to be of either of the two forms

$$E_1(k) = \tfrac{3}{2}v_0^2\delta(k-k_0), \quad E_2(k) = 16(2/\pi)^{\frac{1}{2}}v_0^2k^4k_0^{-5}\exp(-2k^2/k_0^2). \tag{3.3}$$

Here v_0 is the root-mean-square velocity in any direction and the spectra peak is at k_0.

The velocity field is stored as a collection of Fourier amplitudes and synthe-

sized in $\mathbf{x}$ space only along the particle trajectories. In the case of mirror-symmetric turbulence, each realization is taken to be of the form

$$\mathbf{u}(\mathbf{x},t) = \sum_{n=1}^{N} [(\mathbf{b}_n \times \mathbf{k}_n)\cos(\mathbf{k}_n.\mathbf{x}+\omega_n t) + (\mathbf{c}_n \times \mathbf{k}_n)\sin(\mathbf{k}_n.\mathbf{x}+\omega_n t)], \tag{3.4}$$

which automatically gives incompressibility. The vectors $\mathbf{b}_n$ and $\mathbf{c}_n$ are chosen independently from a three-dimensional Gaussian distribution whose variance is chosen to yield the desired v_0. In accord with (3.2), the ω_n are chosen from a Gaussian distribution with standard deviation ω_0. The vectors $\mathbf{k}_n$ are picked from an isotropic distribution such that the desired $E(k)$ would be realized in the limit $N \to \infty$. For E_1, this means that $\mathbf{k}_n$ is isotropically distributed on a sphere of radius k_0. For E_2, each component of $\mathbf{k}_n$ is picked from a Gaussian distribution of standard deviation $\frac{1}{2}k_0$. By the central-limit theorem, the moments of $\mathbf{u}(\mathbf{x},t)$ approach normal values as $N \to \infty$. All the parameters in (3.4) are chosen afresh for each realization.

To realize a normal, maximally helical distribution, the only change is that the coefficient $\mathbf{c}_n \times \mathbf{k}_n$ in (3.4) is replaced by $\pm k_n^{-1}(\mathbf{k}_n \times \mathbf{b}_n \times \mathbf{k}_n)$, where the sign, which determines the sign of the helicity, is kept the same for all the realizations.

The particle trajectories are found by integrating

$$d\mathbf{X}(t)/dt = \mathbf{v}(t), \quad \mathbf{v}(t) = \mathbf{u}(\mathbf{X},t). \tag{3.5}$$

In each realization two particles are followed. One starts at $\mathbf{X}(0) = 0$ and the other at $\mathbf{X}(0) = (\Delta a, 0, 0)$. All the simulations reported here have

$$\Delta a = 10^{-6} k_0^{-1}. \tag{3.6}$$

The strain vector $\partial \mathbf{X}(t)/\partial a_1$ which appears in the formulae of § 2 is evaluated as $\Delta \mathbf{X}(t)/\Delta a$ and the displacement vector $\boldsymbol{\xi}(t)$ is evaluated as the mean of the displacements of the two particles. The averages in the formulae of § 2 are evaluated as averages over R independent realizations. The runs reported here all have

$$N = 20, \quad R = 20\,000. \tag{3.7}$$

Experiments were made to verify that increasing N did not change the results to within the statistical errors. Equation (3.5) is integrated by a fourth-order stable predictor–corrector method due to Hamming (Ralston & Wilf 1960). The starting values are formed by a second-order predictor–corrector scheme and four iterations of Newton's interpolation formulae for the first three time steps. For the runs reported here,

$$\Delta t = 0{\cdot}125(v_0 k_0)^{-1}. \tag{3.8}$$

It was verified by decreasing Δt that errors due to the finite time step were negligible compared with statistical errors.

The Gaussian distributions needed are formed by the log–cosine method (Abramowitz & Stegun 1965) starting with pseudo-random uniformly distributed numbers generated by the RANF congruential routine at the National Center

for Atmospheric Research Computing Facility.† To avoid possible spurious correlation effects, the numbers used are chosen by pseudo-random addressing from a table of 1000 pseudo-random numbers. Each number used from the table is replaced by a new pseudo-random number.

As we shall discuss later, the distribution of $\partial \mathbf{X}/\partial a_1$ becomes highly non-normal during the simulations. In order to estimate in a simple way the errors in the calculated means, we therefore group each run of 20 000 realizations into 40 sets of 500 realizations each. The grand average $\langle z \rangle$ of any quantity z is then

$$\langle z \rangle = \tfrac{1}{40} \sum_{s=1}^{40} \bar{z}_s, \tag{3.9}$$

where the $\bar{z}_s$ are the means over the individual sets of 500. By a central-limit argument, the $\bar{z}_s$ should be approximately normal even though z itself is not. We therefore compute a probable error of the grand average in standard fashion as

$$\delta z = 0{\cdot}6745 \left\{ \tfrac{1}{39} \left[\tfrac{1}{40} \sum_{s=1}^{40} (\bar{z}_s)^2 - \langle z \rangle^2 \right] \right\}^{\frac{1}{2}}. \tag{3.10}$$

4. Results

Simulations were carried out up to $t = 4/v_0 k_0$ and included runs with each of the two choices of spectrum, with helical and mirror-symmetric velocity fields, and with three values of ω_0: $\omega_0 = 0$ (frozen turbulence), $\omega_0 = v_0 k_0$ and $\omega_0 = 2v_0 k_0$. Results with the spectra E_1 and E_2 were similar. The E_1 runs showed somewhat smaller probable errors, however, and it is only these which we present here.

Figure 1 shows $\alpha(t)$ for the maximally helical normal velocity field with $\omega_0 = 0$, $\omega_0 = v_0 k_0$ and $\omega_0 = 2v_0 k_0$, as computed from (2.10). Figure 2 shows the corresponding values of $\eta(t)$ and $\kappa(t)$ as computed from (2.16), (2.5) and (2.12), using

$$\tfrac{1}{2} d[\gamma(t)]^2/dt = \alpha(t)\, \gamma(t) \tag{4.1}$$

with $\gamma(t)$ computed as the Simpson-rule integral of $\alpha(t)$. In these figures, and those to follow, the error bars show probable errors computed by (3.10).‡ For the two non-zero values of ω_0, the plots indicate that both $\alpha(t)$ and $\eta(t)$ settle down to steady-state values after an overshoot which is about 25 % for $\omega_0 = v_0 k_0$ and barely perceptible for $\omega_0 = 2v_0 k_0$. The probable errors increase rapidly with t, largely, as we shall indicate later, because of increasing intermittency of the strain distribution. The wiggles in the curves beyond $t = 3/v_0 k_0$ are due to finite sample size. Similar wiggles appeared, but less rapidly, in the previous work on pure scalar diffusion (Kraichnan 1970).

In the case of the frozen velocity field, both $\alpha(t)$ and $\eta(t)$ show anomalous behaviour. It is not possible to judge from the plots whether $\alpha(t)$ and $\eta(t)$ oscillate, go off to negative infinity or show some other behaviour. It is not economically

† This routine computes successive random integers N_i according to

$$N_{i+1} = (2^{24} - 3)\, N_i \quad (\text{modulo } 2^{48}).$$

We start the routine by taking N_0 as a ten-digit random odd integer.

‡ The bars for $\kappa(t)$ and $\Xi(t)$ are too small to be visible on the plots.

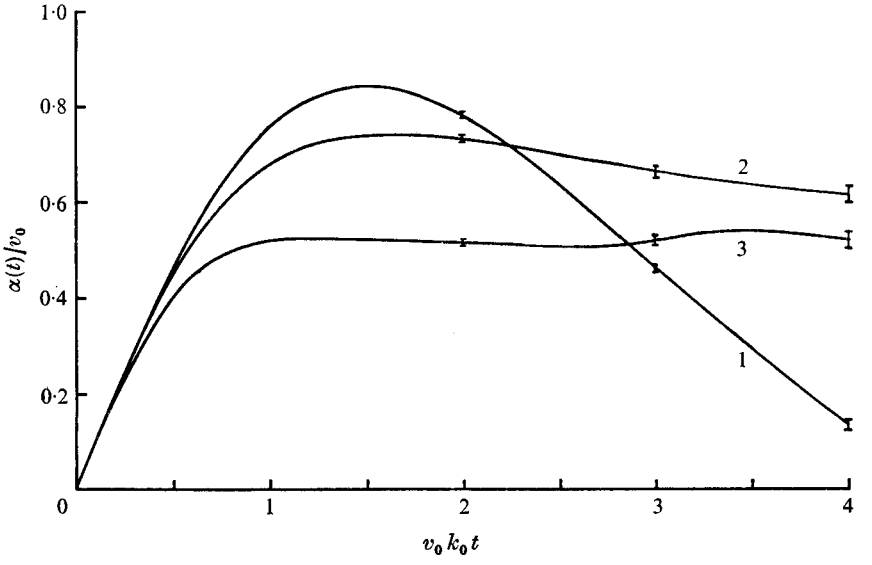

FIGURE 1. The function $\alpha(t)$ for maximally helical normal turbulence. (1) $\omega_0 = 0$, (2) $\omega_0 = v_0 k_0$, (3) $\omega_0 = 2v_0 k_0$.

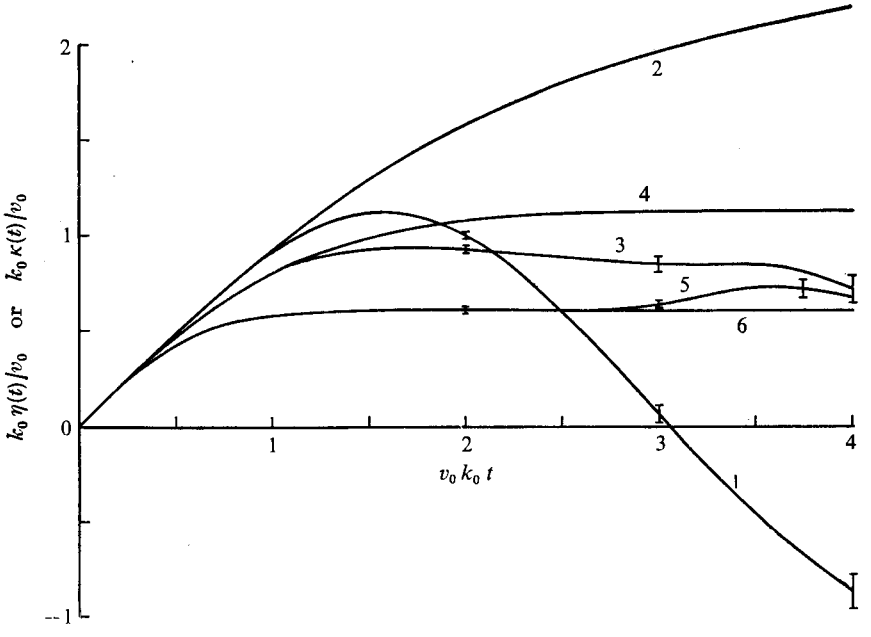

FIGURE 2. The functions $\eta(t)$ and $\kappa(t)$ for maximally helical normal turbulence. (1) $\eta(t)$ for $\omega_0 = 0$, (2) $\kappa(t)$ for $\omega_0 = 0$, (3) $\eta(t)$ for $\omega_0 = v_0 k_0$, (4) $\kappa(t)$ for $\omega_0 = v_0 k_0$, (5) $\eta(t)$ for $\omega_0 = 2v_0 k_0$, (6) $\kappa(t)$ for $\omega_0 = 2v_0 k_0$.

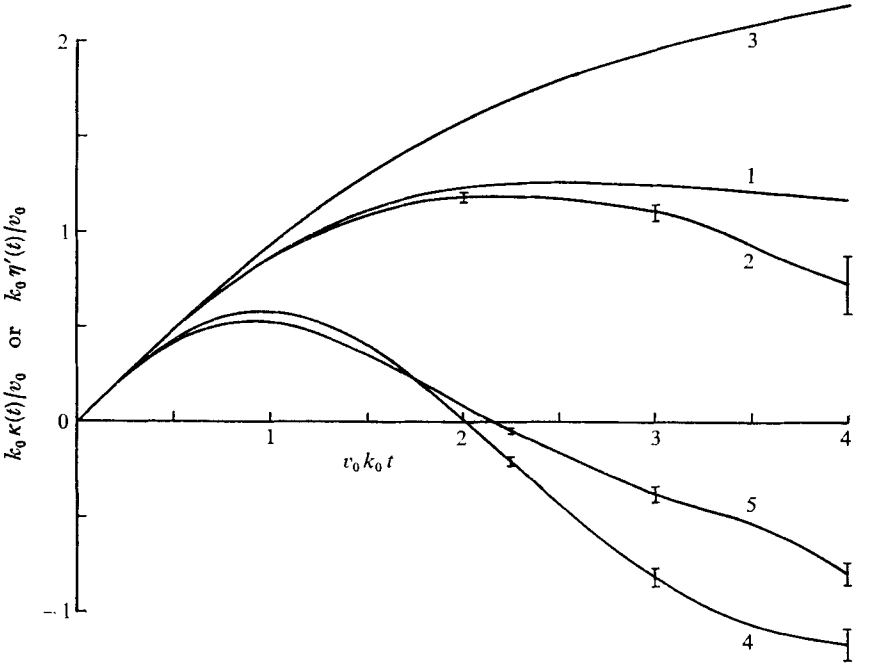

FIGURE 3. The functions $\kappa(t)$ and $\eta'(t)$ for several cases. (1) $\kappa(t)$ for the mirror-symmetric $\omega_0 = 0$ case, (2) $\eta'(t)$ for the mirror-symmetric $\omega_0 = 0$ case, (3) $\kappa(t)$ for the maximally helical $\omega_0 = 0$ case, (4) $\eta'(t)$ for the maximally helical $\omega_0 = 0$ case, (5) $\eta'(t)$ for the maximally helical $\omega_0 = v_0 k_0$ case.

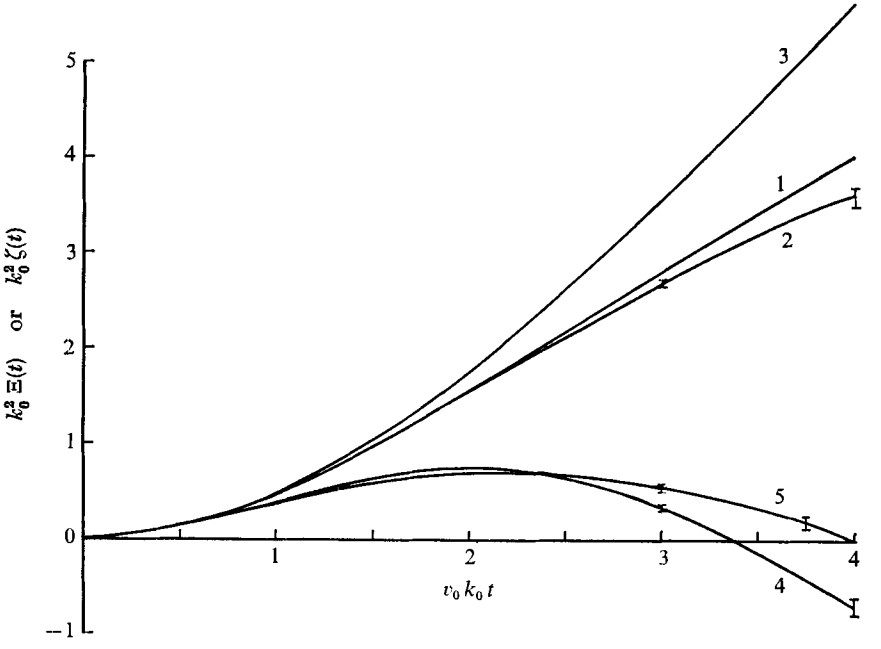

FIGURE 4. The functions $\Xi(t)$ and $\zeta(t)$ for several cases. (1) $\Xi(t)$ for the mirror-symmetric $\omega_0 = 0$ case, (2) $\zeta(t)$ for the mirror-symmetric $\omega_0 = 0$ case, (3) $\Xi(t)$ for the maximally helical $\omega_0 = 0$ case, (4) $\zeta(t)$ for the maximally helical $\omega_0 = 0$ case, (5) $\zeta(t)$ for the maximally helical $\omega_0 = v_0 k_0$ case.

feasible to extend the calculations substantially further in t because the rapid increase in statistical fluctuation with t would require enormous samples.

Figures 3 and 4 compare $\kappa(t)$, $\eta'(t) \equiv d\zeta(t)/dt$, $\zeta(t)$ and $\Xi(t)$ for several of the runs. We note first that the passive-scalar functions $\kappa(t)$ and $\Xi(t)$ are both substantially different in the helical and mirror-symmetric frozen-field cases respectively. Helical turbulence appears clearly to be the better diffuser. The diffusivity in the helical case is nearly twice the mirror-symmetric value at $t = 4/v_0 k_0$ and is still rising. The corresponding curves of diffusivity for $\omega_0 = v_0 k_0$ (not shown here) both level off by $t = 3/v_0 k_0$, with the asymptotic value in the helical case about 40 % higher than in the mirror-symmetric case.

In the mirror-symmetric case, $\eta'(t) = \eta(t)$, and the plot shows remarkably little difference between $\eta(t)$ and $\kappa(t)$. The difference, in fact, is not clearly statistically significant. The curves shown are for the frozen case, in which differences should be most pronounced. The plots for the frozen case serve also to determine $\eta(t)$ and $\kappa(t)$ for a velocity distribution which is piecewise constant in time, over intervals of duration $2\tau_1$, and statistically independent for distinct intervals, thereby giving a velocity correlation time τ_1 (Kraichnan 1976). If the breaks between intervals are at random times in the different realizations, then it is easy to show that

$$[\eta(t)]_{\tau_1} = \begin{cases} (1 - t/2\tau_1)\,\eta(t) + (1/2\tau_1)\int_0^t \eta(s)\,ds & (t \leqslant 2\tau_1), \\ (1/2\,\tau_1)\int_0^{2\tau_1} \eta(s)\,ds & (t > 2\tau_1), \end{cases} \tag{4.2}$$

where the left-hand side is the value for the piecewise-constant case and $\eta(t)$ on the right-hand side is evaluated for the frozen case. Corresponding relations hold for $\eta'(t)$ and $\kappa(t)$. Equation (4.2) follows from the fact that for a given placement of the interval breaks $\eta(t)$ rises from zero at $t = 0$, drops abruptly back to zero at the first (randomly placed) break between intervals and is thereafter periodic with period $2\tau_1$, while reproducing, in each of its rises from zero, the rise of the frozen-field $\eta(t)$ from $t = 0$. It is clear from (4.2) and the plots that the difference between $\eta(t)$ and $\kappa(t)$ in the piecewise-constant mirror-symmetric case is completely negligible for $\tau_1 < 1{\cdot}5/v_0 k_0$.

In contrast, figures 2 and 3 show marked differences among $\eta(t)$, $\eta'(t)$ and $\kappa(t)$ for the maximally helical velocity field, both for $\omega_0 = 0$ and $\omega_0 = v_0 k_0$. The differences are associated with the strong correlation between strain and displacement displayed for the helical case in figure 4. The displacement components ξ_i should be nearly normally distributed, and measurements of kurtosis in the present simulations confirm this (see also Kraichnan 1970). Also, it follows from symmetry that $\langle \partial X_1/\partial a_1 \rangle = 1$. Thus the bending over of the helical $\zeta(t)$ curves into negative values indicates a strong and persistent correlation between strain and displacement, and this shows up in figure 3 as negative values of $\eta'(t)$. Figures 1 and 2 suggest that $\alpha(t)$ and $\eta(t)$ level off at non-zero, positive steady-state values if $\omega_0 > 0$. Equation (2.5) then implies that $\eta'(t)$ should display a negative value which increases in magnitude linearly with t if the plots could be extended to

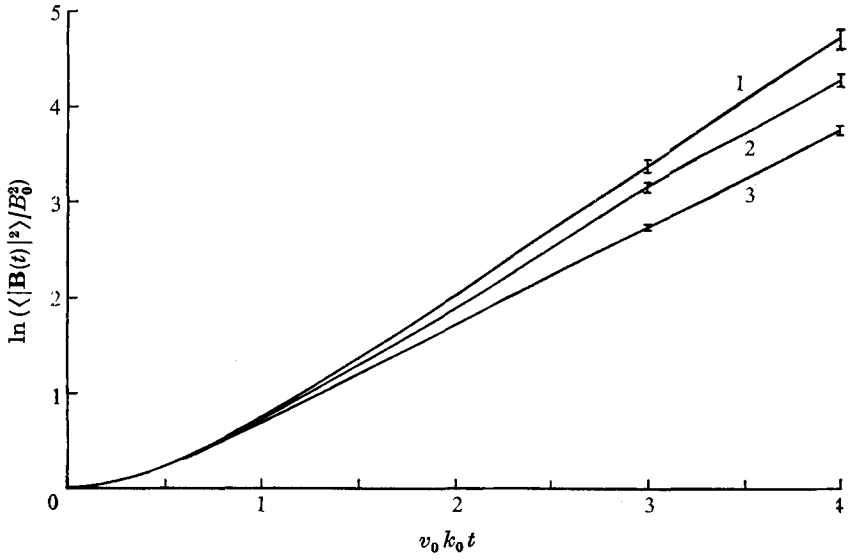

FIGURE 5. Growth of magnetic-field intensity. (1) Mirror-symmetric case with $\omega_0 = 0$, (2) maximally helical case with $\omega_0 = 0$, (3) maximally helical case with $\omega_0 = v_0 k_0$.

large t. It is interesting that the curves for $\eta'(t)$ in the helical case show much less contrast between $\omega_0 = 0$ and $\omega_0 > 0$ than do the curves for $\eta(t)$.

Suppose the initial magnetic field is uniform and has the form

$$\mathbf{B}(\mathbf{x}, 0) = (B_0, 0, 0). \tag{4.3}$$

Then (2.3) gives

$$B_i(\mathbf{X}, t) = B_0 \partial X_i/\partial a_1, \tag{4.4}$$

so that the statistics of $\mathbf{B}(\mathbf{X}, t)$ are just those of $\partial\mathbf{X}/\partial a_1$. In particular,

$$\langle|\mathbf{B}|^2\rangle/B_0^2 = \langle|\partial\mathbf{X}/\partial a_1|^2\rangle, \tag{4.5}$$

$$\langle|\mathbf{B}|^4\rangle/\langle|\mathbf{B}|^2\rangle^2 = \langle|\partial\mathbf{X}/\partial a_1|^4\rangle/\langle|\partial\mathbf{X}/\partial a_1|^2\rangle^2. \tag{4.6}$$

Figures 5 and 6 show the growth of $\langle|\mathbf{B}|^2\rangle$ and $\langle|\mathbf{B}|^4\rangle/\langle|\mathbf{B}|^2\rangle^2$ as given by (4.5) and (4.6) for the helical and mirror-symmetric frozen cases and the helical $\omega_0 = v_0 k_0$ case. It is anticipated theoretically that the strain should show asymptotically exponential growth and that it should become approximately lognormal, thereby displaying ever-increasing intermittency (Batchelor 1959; Cocke 1969; Kraichnan 1974). The plots confirm this expectation. Note that $\langle|\mathbf{B}|^4\rangle/\langle|\mathbf{B}|^2\rangle^2$ is unity at $t = 0$ while its value for a normal distribution in three dimensions, with mean negligible compared with fluctuations, is $\frac{5}{3}$.

Figure 7 shows values of $g(k, t)$ and $g_s(k, t)$ for the helical case with $\omega_0 = 2v_0 k_0$ as computed from (2.22) and (2.25). For $k = 0$, the plotted functions

$$-k^{-2}\ln[g(k, t)], \quad -k^{-2}\ln[g_s(k, t)]$$

reduce simply to $\zeta(t)$ and $\Xi(t)$ respectively. The deviations of the curves for non-zero k from those for zero k in the scalar case are a measure of the deviation

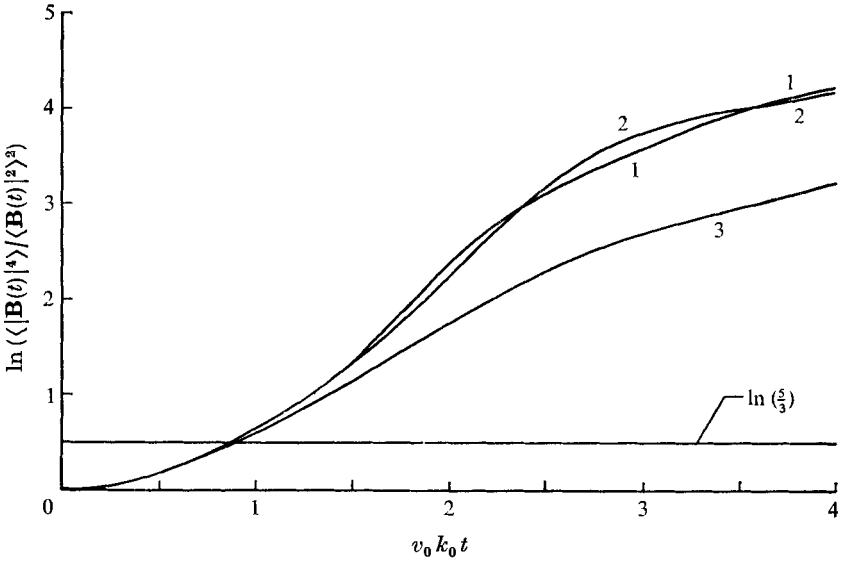

FIGURE 6. Growth of kurtosis of magnetic-field distribution. (1) Mirror-symmetric case with $\omega_0 = 0$, (2) maximally helical case with $\omega_0 = 0$, (3) maximally helical case with $\omega_0 = v_0 k_0$. The horizontal line is at the normal value $\ln \frac{5}{3}$.

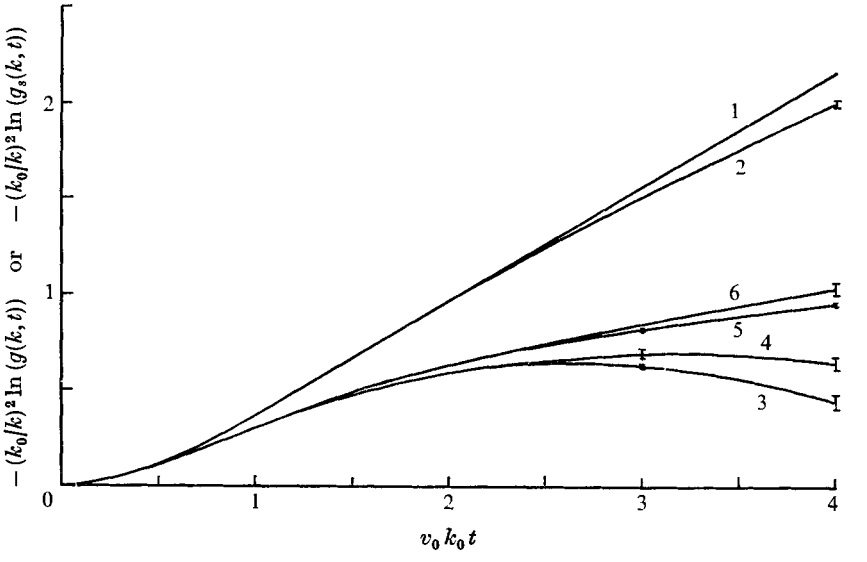

FIGURE 7. The functions $g(k, t)$ and $g_s(k, t)$ for the maximally helical case with $\omega_0 = 2v_0 k_0$. (1) $g_s(k, t)$ at $k = 0$, (2) $g_s(k, t)$ at $k = k_0$, (3) $g(k, t)$ at $k = 0$, (4) $g(k, t)$ at $k = \frac{1}{2}k_0$, (5) $g(k, t)$ at $k = k_0$, (6) the asymptotic expression (2.26) at $k = k_0$.

of the $\boldsymbol{\xi}$ distribution from normality. To see this, we note that if $\mathbf{k}$ in (2.24) were taken along, say, the x_1 axis we should have, noting symmetry,

$$g_s(k, t) = \langle \cos(k\xi_1) \rangle \tag{4.7}$$

instead of (2.25). If ξ_1 is normal we obtain precisely (2.28) if we take account of

isotropy. In the case of $g(k,t)$, interpretation is not so simple. It is of interest to ask for how large a value of k/k_0 the asymptotic small-k form (2.26) is accurate. A plot of (2.26) for $k = k_0$ is included in figure 7, and its deviation from the actual $g(k,t)$ is barely statistically significant. Thus (2.26) seems a good approximation for $k \leqslant k_0$. We did not compute $h(k,t)$.

5. The alpha-squared effect

Although the present calculations are for normal distributions, they serve to test the prediction (Kraichnan 1976) that persistent and extensive helicity fluctuations in mirror-symmetric non-normal turbulence lead to negative values of $\eta(t)$ (the α^2-effect). Consider the following special case of such turbulence. The typical realizations consist of regions large compared with $1/k_0$ in each of which the velocity field is locally homogeneous and isotropic, with maximal helicity. The sign of the helicity changes at random from one region to the next. The transition zones between regions are of thickness $\sim 1/k_0$. Since an ensemble of such realizations has mirror symmetry, $\alpha(t)$ vanishes for the ensemble. Hence the formulae of § 2 give

$$\eta(t) = \eta'(t) = d\zeta(t)/dt, \tag{5.1}$$

where $\zeta(t)$ is given, as before, by (2.7).

Now let t be small enough that most fluid elements have wandered less than the distance to the nearest boundary between regions. Then most elements will experience displacement and strain corresponding to normal, homogeneous, maximally helical turbulence. But $\zeta(t)$, given by (2.7), is invariant to a change of sign of helicity since it is invariant to a mirror-reflexion of the co-ordinate system. It follows that, for such t, simulation values of $\zeta(t)$ in the normal maximally helical cases apply also to the non-normal mirror-symmetric ensemble. The root-mean-square displacement of a fluid element is $(6\Xi)^{\frac{1}{2}}$. Hence the required size of the regions in the mirror-symmetric ensemble for the correspondence to hold can be estimated, for a given t, from figure 4. For $\omega_0 = 0$, $(6\Xi)^{\frac{1}{2}} \sim 6/k_0$ at $t = 4/v_0 k_0$ and $(6\Xi)^{\frac{1}{2}} \sim 3/k_0$ at $t = 2/v_0 k_0$. The latter time is when $d\zeta(t)/dt$ first becomes negative. For $\omega_0 = v_0 k_0$, the corresponding values (not plotted) are $\sim 5/k_0$ and $\sim 3/k_0$.

The characteristic correlation length for the spectrum E_1 can be taken as

$$(3v_0^2)^{-1} \int_0^\infty \langle \mathbf{u}(\mathbf{x}+\mathbf{r}) . \mathbf{u}(x) \rangle \, dr = \pi/2k_0. \tag{5.2}$$

Hence we conclude that the homogeneous results are valid for the present mirror-symmetric ensemble up to $t = 4/v_0 k_0$ provided the locally homogeneous regions in the latter are substantially larger than four correlation lengths. Substantial anomalies in the magnetic diffusivity should appear if the regions are larger than two correlation lengths.

Our results in the maximally helical homogeneous cases $\omega_0 = v_0 k_0$ and $\omega_0 = 2v_0 k_0$ indicate that both $\alpha(t)$ and $\eta(t)$ in these cases approach non-zero asymptotic values at large t. Then (2.5) implies that $d\zeta(t)/dt$ is negative at large t with a magnitude that grows linearly with t. Thus, if the regions are large

enough, as large a negative value of $\eta(t)$ as desired can be realized in the locally homogeneous mirror-symmetric ensemble.

So far we have assumed that the sign of the helicity in a given region persists forever. We can generalize the locally homogeneous ensemble by introducing a helicity correlation time τ_2 which is realized as follows. The ensemble as described above persists over intervals of duration $2\tau_2$ during which the region boundaries and the signs of helicity in the regions are constant. But on distinct intervals the locations of the regions and the signs of helicity are statistically independent. Moreover, the transition times between the intervals are randomly staggered in different realizations. With this change, the homogeneous, maximally helical values of $\eta'(t) = d\zeta(t)/dt$ from the simulation runs are related to the locally homogeneous mirror-symmetric values of $\eta(t)$ by

$$\eta(t) = \begin{cases} (1-t/2\tau_2)\,\eta'(t) + (1/2\tau_2)\displaystyle\int_0^t \eta'(s)\,ds \quad (t \leqslant 2\tau_2), \\ (1/2\tau_2)\displaystyle\int_0^{2\tau_2} \eta'(s)\,ds \quad (t > 2\tau_2), \end{cases} \tag{5.3}$$

in analogy with (4.2). This relation holds, both for zero and for non-zero ω_0, provided the locally homogeneous regions are larger than the migration distance of most fluid elements in the time $2\tau_2$. By making the regions large enough with, say, $\omega_0 = v_0 k_0$, we can realize as large a negative steady-state value of $\eta(t)$ as desired in the locally homogeneous ensemble.

6. Discussion

Our principal results are that, first, in maximally helical, isotropic, homogeneous, normal turbulence with $\omega_0 \sim v_0 k_0$, the magnetic diffusivity $\eta(t)$ and alpha-effect coefficient $\alpha(t)$ tend to non-zero, finite steady-state values. Second, in mirror-symmetric, homogeneous, isotropic turbulence with, again, a correlation time $\sim 1/v_0 k_0$, $\eta(t)$ differs from the passive-scalar diffusivity $\kappa(t)$ by a negligible amount for all t. These results follow either directly from the simulations for non-zero ω_0 or from the frozen ($\omega_0 = 0$) simulations together with (4.2), which relates frozen-field results to piecewise-constant results. A corollary of the first principal result is that the α^2-effect, the development of negative $\eta(t)$ in mirror-symmetric turbulence with persistent helicity fluctuations, occurs for $\omega_0 \sim v_0 k_0$.

These results extend to more realistic correlation times the predictions of quasi-linear theory, which are valid for $\omega_0 \gg v_0 k_0$ (Steenbeck & Krause 1969; Roberts 1971; Kraichnan 1976). That approximation gives $\eta(t) = \kappa(t)$ in normal turbulence and yields values which are identical for the helical and mirror-symmetric cases. With the time correlation (3.2) the asymptotic steady-state quasi-linear values for maximal helicity are

$$\eta(\infty) = \kappa(\infty) = (\tfrac{1}{2}\pi)^{\frac{1}{2}} v_0^2/\omega_0 = \alpha(\infty)/k_0. \tag{6.1}$$

Thus no steady state is reached for $\omega_0 = 0$. For $\omega_0 = v_0 k_0$, the quasi-linear value exceeds the steady-state values suggested by the simulations by $\sim 40\,\%$ for the

mirror-symmetric $\kappa(\infty)$, by $\sim 10\,\%$ for the maximally helical $\kappa(\infty)$, by $> 50\,\%$ for the maximally helical $\eta(\infty)$ and by $> 100\,\%$ for the maximally helical $\alpha(\infty)$. At $\omega_0 = 2v_0 k_0$, these overestimates are reduced to excess of $\sim 5\,\%$ for $\kappa(\infty)$ and $\eta(\infty)$, which are nearly the same in the maximally helical and mirror-symmetric cases and nearly equal to each other, and $\sim 20\,\%$ for the maximally helical $\alpha(\infty)$.

The direct-interaction approximation for the normal mirror-symmetric case gives identical values for $\kappa(t)$ and $\eta(t)$. Also, it gives the same value for $\kappa(t)$ in both the mirror-symmetric and the maximally helical case (Roberts 1975; Kraichnan 1976). In contrast to the quasi-linear approximation, it gives remarkably accurate values for mirror-symmetric $\kappa(t)$ both for $\omega_0 = 0$ and $\omega_0 \sim v_0 k_0$, and at all t. Its error for $\eta(t)$ in the mirror-symmetric cases and for $\kappa(t)$ in the maximally helical cases then reduces to the differences between the true values of these functions and those of the mirror-symmetric $\kappa(t)$. The direct-interaction equations for magnetic Green's functions and $\eta(t)$ in the maximally helical case and for $\alpha(t)$ (Lerche 1973) have not been integrated numerically. However, we expect that they do not give identical values for $\eta(t)$ and $\kappa(t)$, in contrast to the quasi-linear approximation. The reason is that these equations give a coupling between $g(k,t)$ and $h(k,t)$, with the result that the equation for $g(k,t)$ is not the same as the direct-interaction equation for $g_s(k,t)$. This is a most interesting situation because the direct-interaction approximation uses the coefficients in the perturbation expansions of $g(k,t)$ and $g_s(k,t)$ only up to terms in t^2, and the two functions are identical to this order.

An unanticipated result of the simulations is the large difference exhibited between values of $\kappa(t)$ for the mirror-symmetric and maximally helical cases. It is not even certain from the curves presented that $\kappa(t)$ approaches a steady-state value at large t in the frozen, maximally helical case, although it clearly does in the frozen, mirror-symmetric case (Kraichnan 1970). In the latter case, the displacement $\boldsymbol{\xi}$ was found to stay close to a normal distribution, as measured by kurtosis, out to $t = 15/v_0 k_0$, with a dip of about 12 % below the normal value of kurtosis in the neighbourhood of $t = 3/v_0 k_0$. In the present maximally helical simulation, the kurtosis is 20 % below the normal value at $t = 4/v_0 k_0$ and is still slowly falling. The physical reasons for this behaviour, and for the possibly associated anomalies in $\alpha(t)$ and $\eta(t)$ in the frozen, maximally helical case, need to be elucidated by further theoretical and numerical work. We should note that in all the simulations reported here the velocity field along the trajectories shows a kurtosis within 1 % of the normal value at all t. This is the order of deviation expected on the basis of the sample size of 20 000.

We noted earlier that when $k \ll k_0$ the coefficients of an expansion in powers of k of the response-function formulae (2.22), (2.23) and (2.25) must agree with the coefficients of the expansions of the asymptotic formulae (2.26)–(2.28), provided t is large enough that the higher terms in the expansions are not negligibly small. This means that t must be large enough that the response functions differ appreciably from their values at $t = 0$, thus that $t \gg 1/v_0 k_0$.

In the case of $g_s(k,t)$ this implies that $\boldsymbol{\xi}$ is normally distributed for such t, a fact that is most easily seen by comparing (2.28) with the alternative form (4.7) instead of (2.25). The normality of $\boldsymbol{\xi}$ for large t is a central-limit behaviour

associated with the fact that ξ is then a sum of many contributions:

$$\xi = \sum_s \xi_s, \tag{6.2}$$

where each ξ_s comes from an independent eddy if $\omega_0 \lesssim v_0 k_0$ or from an independent correlation interval if $\omega_0 \gg v_0 k_0$.

In the case of $g(k,t)$, it is convenient to use instead of (2.22) the isotropically equivalent form

$$g(k,t) = (\partial X_1/\partial a_1)\cos(k\xi_2). \tag{6.3}$$

Suppose there is mirror-symmetry so that $\gamma(t)$ vanishes. The equivalence of (2.26) and (6.3) at order k^2 gives the identity $\zeta(t) = \zeta(t)$. At order k^4, with isotropy taken into account, it gives

$$\langle(\partial X_1/\partial a_1)\,\xi_2^4\rangle = 3\langle(\partial X_1/\partial a_1)\,\xi_2^2\rangle^2, \tag{6.4}$$

which may be compared with the corresponding normality relation

$$\langle \xi_2^4\rangle = 3\langle \xi_2^2\rangle^2 \tag{6.5}$$

which arises at order k^4 from the equality of the two expressions for $g_s(k,t)$.

The strain $\partial X_1/\partial a_1$ at large t is the resultant of independent stretchings or shrinkings in each eddy or independent time interval. Consequently (cf. Cocke 1969; Kraichnan 1974) it has the form

$$\partial X_1/\partial a_1 = \prod_s w_s, \tag{6.6}$$

where the w_s are independent. Now let s range over a large number N of similar eddies and let

$$\alpha = \langle w_s(\xi_2)_s^2\rangle, \quad \beta = \langle w_s\rangle, \quad \theta = \langle w_s(\xi_2)_s\rangle. \tag{6.7}$$

Homogeneity requires $\beta = 1$ and isotropy requires $\theta = 0$. Following a procedure like the standard one for demonstrating (6.5) from (6.2) as $N \to \infty$, we have

$$\langle(\partial X_1/\partial a_1)\,\xi_2^2\rangle = N\beta^{N-1}\alpha, \quad \langle(\partial X_1/\partial a_1)\,\xi_2^4\rangle = 3N^2\beta^{N-2}\alpha^2, \tag{6.8}$$

both with fractional error of order $1/N$. Thus, noting $\beta = 1$, we get (6.4) as $N \to \infty$. Similar manipulations verify the higher relations obtained by comparing (6.3) and (2.26).

If $\beta = 1$ and w_s fluctuates, then $\langle w_s^2\rangle > 1$. Thus (6.6) gives

$$\langle(\partial X_1/\partial a_1)^2\rangle = \langle w_s^2\rangle^N, \tag{6.9}$$

where the right-hand side grows exponentially with N. In contrast to this exponential growth, (6.8) shows that $\langle(\partial X_1/\partial a_1)\,\xi_2^2\rangle$ grows only linearly with N. The physical reason behind this is that the fluid elements suffer many random rotations during their migration. In effect, memory of initial orientation decays exponentially at the same time as the magnitude of the strain increases exponentially. The net result is the slow, linear growth of $\zeta(t)$, with equal contributions, on the average, from each eddy traversed.

The asymptotic lognormality of $\partial X_1/\partial a_1$ implies increasing intermittency of the **B** distribution, as we have discussed in connexion with figures 5 and 6. At the same time $\langle|\mathbf{B}|^2\rangle$ grows exponentially. This means that great care must

be exercised in applying the weak-magnetic-field equations to physical problems. The fluctuating Lorentz forces can rapidly become strong locally even when the mean value $\langle|\mathbf{B}|^2\rangle$ indicates weak Lorentz forces. Both the cascade of magnetic field fluctuations to smaller scales and the Ohmic dissipation will play crucial roles in determining the magnitude and distribution of the Lorentz forces in a physical application.

This work was supported by the National Science Foundation under Grant OCD75-15100 and by the Office of Naval Research under Contract N00014-67-C-0284. The computations were performed at the National Center for Atmospheric Research. I am grateful to Sandra Fuller for programming assistance.

REFERENCES

ABRAMOWITZ, M. & STEGUN, I. A. 1965 *Handbook of Mathematical Functions*, p. 953. Dover.

BATCHELOR, G. K. 1959 *J. Fluid Mech.* **5**, 113.

COCKE, W. J. 1969 *Phys. Fluids*, **12**, 2488.

KRAICHNAN, R. H. 1970 *Phys. Fluids*, **13**, 22.

KRAICHNAN, R. H. 1974 *J. Fluid Mech.* **64**, 737.

KRAICHNAN, R. H. 1976 *J. Fluid Mech.* **75**, 657.

LERCHE, I. 1973 *J. Math. Phys.* **14**, 1579.

MOFFATT, H. K. 1974 *J. Fluid Mech.* **65**, 1.

RALSTON, A. & WILF, H. S. 1960 *Mathematical Methods for Digital Computers*, p. 100. Wiley.

ROBERTS, P. H. 1971 In *Lectures in Applied Mathematics* (ed. by W. H. Reid). Philadelphia: Am. Math. Soc.

ROBERTS, P. H. 1975 *Magnetnaya Gidrodinamika*, no. 2, p. 3.

STEENBECK, M. & KRAUSE, F. 1969 *Astron. Nachr.* **291**, 49.